Pergamon PII: S0016-0032(96)00101-9

J. Franklin Inst. Vol. 334B, No. 3, pp. 337–356, 1997

Published by Elsevier Science Ltd
Printed in Great Britain
0016-0032/97 $17.00+0.00

Design of a Permanent/Electromagnetic Magnetic Bearing-controlled Rotor System

by YI-HUA FAN *and* AN-CHEN LEE

Department of Mechanical Engineering, National Chiao Tung University, Taiwan, R.O.C.

and FOAM-ZONE HSIAO

Synchrotron Radiation Research Center, Taiwan, R.O.C.

(Received 24 July 1996; accepted 11 September 1996)

ABSTRACT: *This study proposes design procedures for the permanent-magnet-biased magnetic bearings (PEMBs) in rotor systems. Many aspects of designing magnetic bearings are discussed, e.g. the selection of a permanent magnet material, dimensions of electromagnets and permanent magnets, gap length, load capacity and maximum Ampere-turns. Linearization and DC current driver are the two constraints for determining feasible designs. According to an analytical model with a rigid body assumption for the rotor-bearing system, a decentralized output feedback control algorithm is employed to control this inherently unstable magnetic suspension rotor system. Experimental results indicate that the controlled rotor performs well at rotor speeds up to* 12,000 *rpm.*

I. Nomenclature

A_g	effective cross-sectional area of the air gap
B_{sat}	saturation flux density of the material of EM
B_p, H_p	flux density and field strength of PM
b, p	dimensions of PM in the axial and radial directions
d_c	diameter of coil wire
d_i, d_o, L_{em}	inner diameter, outer diameter and axial length of the motor stator
d_m	diameter of inner sleeve
d_n	change of air gap length, $n = 1 \sim 8$
d_r	shaft diameter
d_s	outer diameter of the laminated sleeve
EM	electromagnet
F	magnetic force
F_{ext}	maximum external force
F_{em}	electromagnetic force provided by current with EM as the only source, i.e. not biased by PMs
F_{min}	minimum desired magnetic force

F_n	electromagnetic force, $n = 1 \sim 8$
G	air gap
g	acceleration of gravity, 9.81 m/s^2
i_{max}	maximum coil current
i_n	coil current corresponding to electromagnet n, $n = 1 \sim 8$
J	polar moment of inertia of shaft cross-section
k_i, k_d	current and displacement stiffness of magnetic bearing
k_{pj}, k_{dj}	position and velocity feedback gain, $j = 1 \sim 4$
L	distance between the rotor mass center and the MB
L_m, w_m	length and width of the pole rib
MB	magnetic bearing
m, I_r, I_a	mass, transverse and polar mass moment of inertia of the rotor
N	number of coil turns
PEMB	permanent/electromagnetic magnetic bearing
PM	permanent magnet
T_{max}	maximum applied torque
W	load capacity
w_p	effective width of the pole face
w_r	width of stator ring and outer sleeve ring
x, y	displacements and angular displacements of the rotor mass center
θ_x, θ_y	
x_1, x_2	displacements of the rotor at locations of MBs
y_1, y_2	
ε, η	reluctance and leakage factor
μ_0	permeability of free space
$\phi_{e,max}$	maximum coil-provided regulating flux
ϕ_{max}	maximum flux
ϕ_p	PM-induced flux
Ω	rotating speed of the rotor

II. Introduction

Magnetic bearings (MBs) have found extensive applications in industrial rotating machines in the recent decade. MB applications are primarily in non-contact features between the rotor and the bearing and in active vibration control of the rotor shaft. In a rotor-bearing system, two kinds of MBs (distinguished by the direction of the acting bearing forces) are commonly used: radial type and axial type MBs. Unlike conventional bearings, MBs can be used to change the stiffness and damping coefficient of the overall rotor-bearing system by a suitable control method. Control methods used for actively controlling a rotor include the conventional PD, PID, PIDD control (**1**–**3**), modern optimum regulation control (LQG/LQR) (**4**) and nonlinear sliding mode control. Signals of the feedback loop may include the position, velocity or acceleration of the shaft. Furthermore, observers can be constructed to estimate the velocity or acceleration signals in cases where suitable sensors are unavailable (**2**). When using MBs as force actuators, a large amount of bias current is commonly provided to the coils of the electromagnets (EMs) to retain the linearity between the bearing forces and the coil control current. However, this approach unavoidably consumes a large amount of electric power. An alternative approach to solve this problem involves using per-

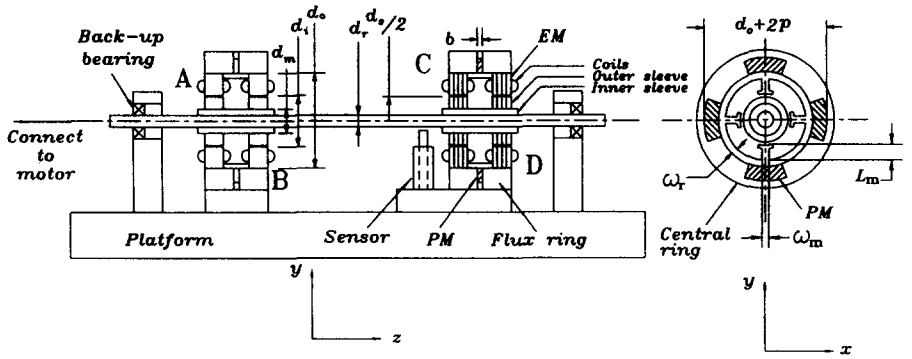

FIG. 1. Configuration of the PEMB controlled rotor system.

manent magnets (PMs) to provide the required bias flux field at the expense of a more precise alignment.

Lee *et al.* (**5, 6**) proposed a rotor supported by the permanent/electromagnetic magnetic bearing (PEMB) to operate well under the control of four simple analog PD controllers. In this study, the design considerations of the PEMBs and the method for analyzing the complete rotor-bearing system are presented. Also, a decentralized output feedback control algorithm is used to simplify the controller design and implementation.

III. The PEMB Controlled Rotor-Bearing System

Figure 1 shows the configuration of the PEMB controlled rotor-bearing system. The rotor is suspended by two sets of PEMBs; a motor to regulate the rotor's speed is connected at one end of the shaft through a flexible coupling, thereby eliminating the requirement for an axial-type MB (**1, 7–9**). Each PEMB consists of a PM part and two EM parts; the main flux field in the air gap is provided by the PM; meanwhile, the EMs are used to regulate the strength of the flux. The PM part, which contains four arch-shaped permanent magnets, where these four permanent magnets form short sections of a circular ring, is located between two orthogonal disposed pole sets of EMs. To reduce the flux leakage between PMs, the central ring must be made of a non-magnetic material, where aluminum alloy is used here. Each EM's stator is a four-pole stator wound with the same number of turns of control coil. Each stator and journal are constructed by a stack of ferromagnetic laminations. For such a MB configuration, the PM flux takes the loop parallel to the shaft axis, and the EM flux circulates along the loop perpendicular to the shaft axis without passing through the PMs. Hence, the flux through the air-gap between the pole face and the rotor periphery is the combination of the bias flux from the PMs and the flux from the EMs (**5**). For each PEMB's control circuit (Fig. 2), the coils along each axis are connected in a series and independently excited by the vertical and horizontal control currents. Each direction of a control current is supplied by a bi-directional current driver and, consequently, two current drivers per PEMB are necessary. Also, two eddy current sensors are used for obtaining the journal displacement in the horizontal and vertical directions, respectively; the measured signals are fed into two analog PD controllers. Moreover, to support the

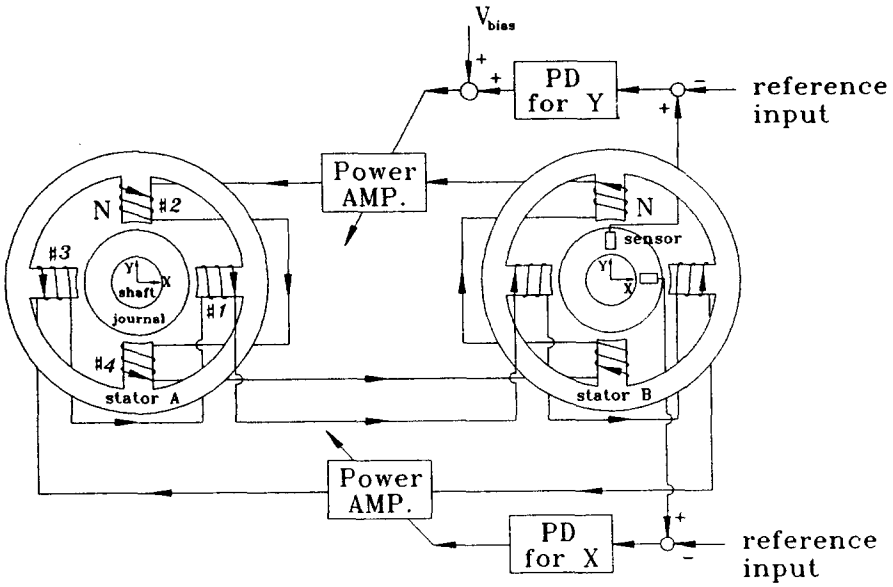

FIG. 2. Control circuit for a PEMB.

rotor weight, an additional constant voltage is applied in the vertical direction coils to provide the required static control current.

When the rotor deviates from the concentric position by a small amount, the non-uniform distribution of the air-gap flux leads to a non-zero resultant magnetic force acting on the rotor in the deviation's direction. The rotor position can be controlled by feeding the EM coils with an amount of current proportional to the amount of deviation in such a manner that the flux in the narrowed-side air gap is reduced; meanwhile that in the widened-side is increased. Thus, the net force produced by the combined flux can be controlled by the coil current and is a function of the rotor displacement and coil current.

IV. Design Considerations

Designing a PEMB involves three specifications: the load capacity, stiffness and damping. The latter two specifications are related to designing the control algorithm. In the main-body design, only the specification of load capacity must be considered. The so-called main-body refers to a PEMB with the controller excluded. The flow chart in Fig. 3 clearly outlines the detailed design procedures for determining the main parameters of a PEMB. Designing the proposed PEMBs is thoroughly discussed in the following.

Step 1. *MB configuration*

The configuration shown in Fig. 1 is adopted here. For this type of PEMB, at least four poles are required since the EM flux circulates along the half circle path. Each pole may contain more than one rib to increase the load capacity. The adopted

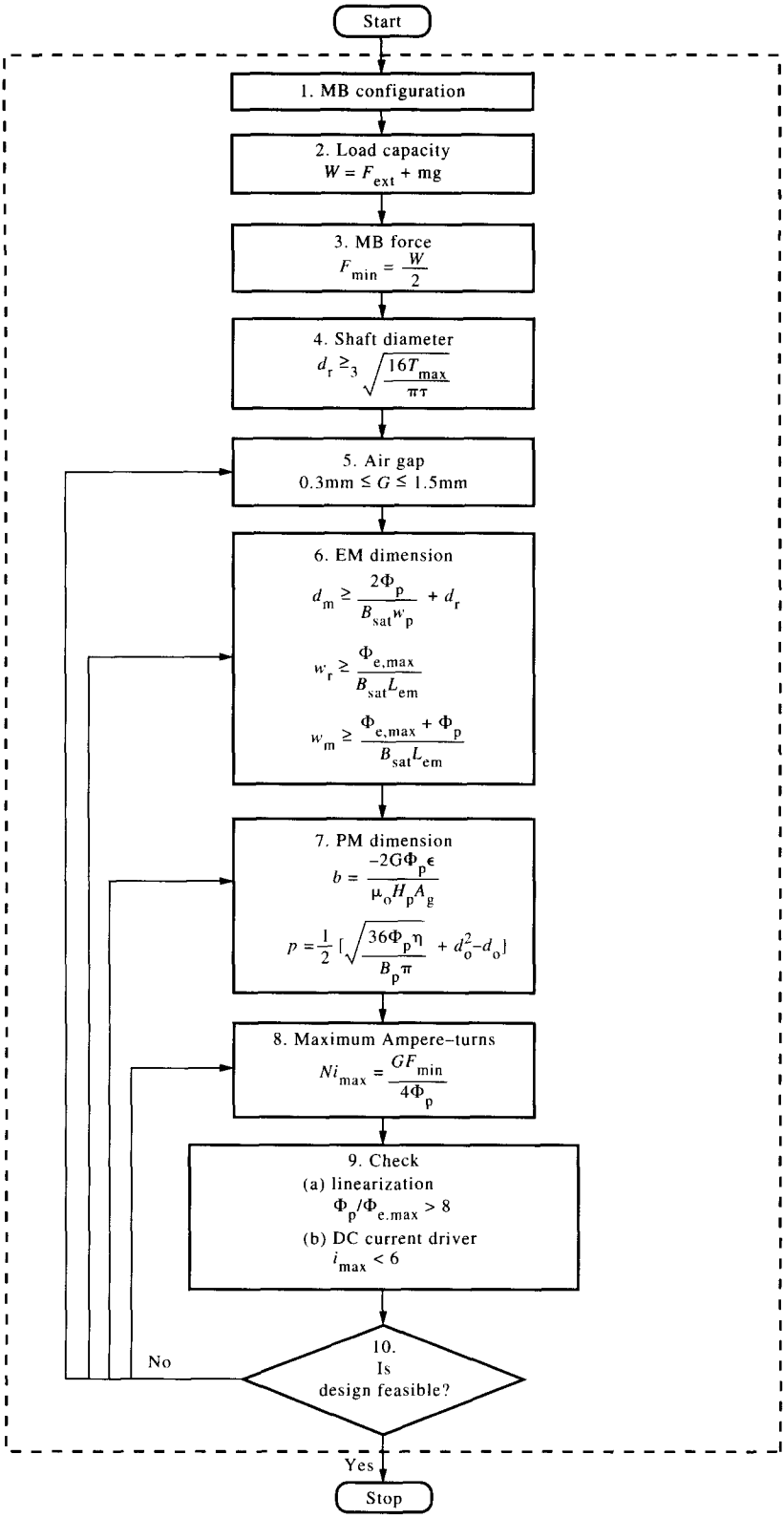

FIG. 3. Flow chart for the PEMB design.

configuration with the winding scheme shown in Fig. 2 is uncoupled for the vertical and horizontal directions of bearing forces. The direction of flow of the PM flux converges to the rotor's center for one stator and diverges from it for another. This winding scheme will, for example, strengthen the total flux of the top air gaps for both stators and weaken that for the bottom air gaps when the rotor moves downward. Thus, the magnetic forces generated are directed upward for both stators.

Step 2. *Load capacity*

Selecting load capacity W is based on practical requirements and is the sum of the rotor weight mg and the allowable external force F_{ext}. The symbol F_{ext} refers to the maximum external force allowed on the rotor, and not the magnetic force by the two PEMBs; furthermore, F_{ext} contains both static and dynamic components. The load capacity used here as a reference value is 100 N.

Step 3. *MB force*

The general formula for the magnetic force is

$$F\frac{8\phi_p}{\phi_e}F_{em} \tag{1}$$

where ϕ_p is the PM-induced flux in the air gap region, ϕ_e is the coil-provided regulating flux due to the EMs, and F_{em} is the electromagnetic force provided by current when the air is not premagnetized by the PM (**5**).

The required magnetic force of both MBs can be determined according to the load capacity and the position of MBs. The external force is assumed here to be applied at the middle point of the shaft so that the required magnetic force for both MBs are the same and equal to half of the load capacity. Thus, the minimum desired magnetic force F_{min} must be equal to the required magnetic force, expressed as:

$$F_{min} = \frac{W}{2}. \tag{2}$$

As the minimum desired magnetic force is determined, the maximum coil-provided regulating flux and the PM-provided bias flux can be determined. A detailed description is given in Step 6.

Step 4. *Shaft diameter*

The type of application and what stress strength is required must be considered since the state's primary function of the shaft is to transmit the driver energy when selecting the shaft diameter d_r. The stress produced in the shaft as a result of transmitting driver energy is torsional. A simple technique for sizing rotor shaft is based on the maximum torsional stress τ expressed in the following.

$$\tau \geqslant \frac{T_{max}\, d_r/2}{J} \tag{3}$$

where T_{max} is the maximum torque applied in the shaft and J is the polar moment of inertia of shaft section.

Thus, the shaft diameter can be determined as

$$d_r \geqslant \sqrt[3]{\frac{16T_{max}}{\pi\tau}}. \tag{4}$$

Furthermore, in sizing the shaft, the effects of key stress, shaft deflection and fatique must be considered. The details can be seen in Ref. (**6**).

Step 5. *Air gap*

Reducing the gap length not only enlarges the bearing load capacity, but also increases the precision requirements for manufacturing and alignments and, consequently, increase the bearing's cost. In selecting the air gap G, to retain the linear characteristics of the PEMB, the maximum radial displacement of the controlled rotor is generally maintained within one tenth of the nominal air gap size which usually ranges from 0.03 to 0.15 mm (**7**).

Step 6. *EM dimensions*

The common stator (EM) is similar to an electric motor stator made of laminated silicon steel strips, where the lamination reduces the eddy current effect. The pre-arranged dimensions of the stator, i.e. L_{em}, A_g and L_m, are given as follows:

$$\begin{aligned} L_{em} &= \text{axial length} = Q \cdot w_s, \\ A_g &= \text{cross-sectional area of the air gap,} \\ &= w_p \cdot L_{em}, \\ L_m &= \text{length of the pole rib,} \end{aligned}$$

where Q is the number of silicon steel strips and w_s the thickness per strip. Because the eddy current effect depends on the squares of thickness of laminations (**10**), w_s should be as small as possible; the thickness used here is 0.5 mm. The symbol w_p refers to the pole face's effective width.

The other dimensions of the stator and rotor of EMs should be determined by the constraint since the maximum flux ϕ_{max} flowing through any section of the stator and rotor must be less than the corresponding saturation flux ϕ_{sat}. The value of ϕ_{max} is composed of the PM-provided bias flux and the maximum coil-provided regulating flux $\phi_{e,max}$, can be calculated as follows:

The electromagnetic force for the current when the air is not premagnetized by the PM is

$$F_{em} = \frac{\phi_e^2}{2\mu_0 A_g} \tag{5}$$

where μ_0 is the free space's permeability.

According to Eqs (1), (2) and (5) and the linearization relationship between the magnetic force and control current (**5**), the maximum coil-provided regulating flux can be determined as

$$\phi_{e,max} > \sqrt{\frac{\mu_0 A_g F_{min}}{32}}. \tag{6}$$

When the maximum coil-provided regulating flux is determined, the choice of ϕ_p can be determined by the desired magnetic force and maximum coil-provided regulating flux, expressed as:

$$\phi_p = \frac{\mu_0 A_g F_{min}}{4\phi_{e,max}}. \tag{7}$$

According to the constraint on magnetic saturation, the diameter of inner sleeve d_m (Fig. 1), the width of stator ring and outer sleeve ring w_r and the width of pole rib w_m can be determined as

$$d_m \geqslant \frac{2\phi_p}{B_{sat} w_p} + d_r, \tag{8}$$

$$w_r \geqslant \frac{\phi_{e,max}}{B_{sat} L_{em}}, \tag{9}$$

$$w_m \geqslant \frac{\phi_{e,max} + \phi_p}{B_{sat} L_{em}}. \tag{10}$$

The above three dimensions are suggested to be chosen at their lower bounds to cause the final design to become a compact device.

The other dimensions of EMs (including the outer diameter of laminated sleeve d_s, the inner diameter of the stator d_i and the outer diameter of the stator d_o), can be determined as follows:

$$d_s = d_m + 2w_r, \tag{11}$$

$$d_i = d_s + 2G, \tag{12}$$

$$d_o = d_i + 2L_{em} + 2w_r. \tag{13}$$

Step 7. PM dimensions

Before determining the PM's dimensions, the material to be used in the PMs should be first determined. Figure 4 shows the typical demagnetization curves of some permanent magnet materials. The development of permanent magnets has made it possible to provide field strengths sufficiently strong for MB applications. For instance, the Alnico series of PMs can provide a flux density as high as 1.35 Tesla. However, an additional requirement that a linear demagnetization curve coincide with the recoil curve further narrows the range of PM candidates. The desired demagnetizing characteristics of the PM materials allow the PM material to be magnetized before the complete PEMB is constructed without losing the PM's field strength. When using PMs, the preferable situation is to allow the PMs' field strength to be their maximum energy product value so that the utilization of PMs is most effective; that is, the product of the field strength of PM, H_p, and the flux density, B_p, reaches the maximum value. Under these considerations, the rare earth material NdFeB was chosen as our PM material. In this

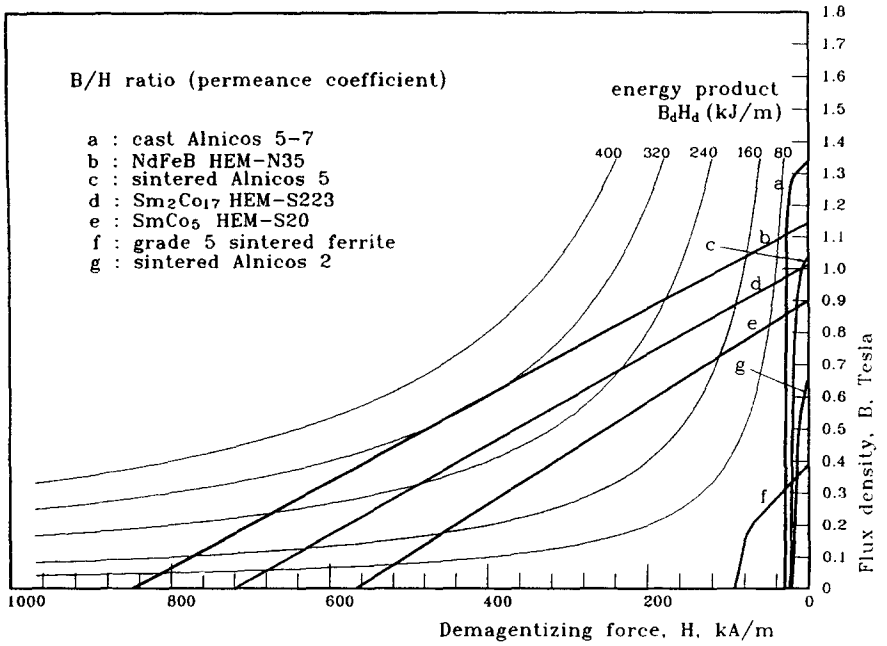

FIG. 4. Demagnetization curves of some permanent magnet materials.

PEMB prototype, the designed working point (H_p, B_p) on the demagnetization curve of the NdFeB PM is chosen to be slightly above the maximum energy product value on account of the unavoidable leakage flux along the PM flux path.

The dimensions of the arch-shaped permanent magnet in the axial and radial directions are, respectively (**5**),

$$b = \frac{-2G\phi_p\varepsilon}{\mu_0 H_p A_g}, \tag{14}$$

$$p = \tfrac{1}{2}\left[\sqrt{\frac{36\phi_p\eta}{B_p\pi} + d_o^2} - d_o\right]. \tag{15}$$

In these equations, the derivation of the axial thickness b is based on the application of Ampere's circuit law to the PM's flux path. Meanwhile that of the radial thickness p is based on the fact that the span angle of the arch-shaped permanent magnet is 40° along the circumferential direction adopted here. Notably, this procedure of designing PM dimensions can be extended to other PM configurations.

In the above equations, the reluctance factor ε is adopted on account of the imperfect joints and the slight reluctance in the pole pieces; the leakage factor η is for the unavoidable leakage flux. The values of ε and η can be calculated using detailed and complex methods, such as permeance analysis (**5**). In most cases, $\varepsilon = 1.2$ and $\eta = 3$ can be adopted.

Step 8. *Maximum Ampere-turns*

When determining the value of the maximum number of Ampere-turns, the magnetic flux density of the pole pieces must not be allowed to reach the saturation level. The maximum Ampere-turns is determined by the PEMB's load capacity, gap size and PM supported bias flux. Since each PEMB should provide the minimum desired magnetic force when the coils in the corresponding direction carry the maximum current i_{max}, by summing the two magnetic forces caused by magnetization in the air gaps in the opposite directions and then equalizing with the minimum desired magnetic force, we can relate the maximum Ampere-turns to F_{min}, G and ϕ_p by the expression (**5**)

$$Ni_{max} = \frac{GF_{min}}{4\phi_p}. \tag{16}$$

The maximum current can be determined once the number of coil turns N winding around each pole is properly chosen.

If the coil is made of copper, then the diameter d_c of the coil wire would be determined by the maximum coil current and the current load capacity of the copper wire q. The value of d_c can be calculated as

$$d_c = \sqrt{\frac{4i_{max}}{\pi q}}, \tag{17}$$

where $q = 6$ A/mm^2 is used in our design.

Step 9. *Check linearization and DC current driver*

(*a*) *Linearization.* Linearization of the relationship between the magnetic force and control current is the paramount goal of pre-magnetization. To ensure that the relationship is linear, the following inequality must hold (**5**):

$$\frac{\phi_p}{\phi_{e,max}} > 8. \tag{18}$$

(*b*) *DC current driver.* As mentioned in section III, such a PEMB construction requires a bi-directional DC driver. The maximum control current must be less than the nominal current provided by the DC driver, thus, an additional constraint due to the DC current driver in our design is

$$i_{max} < 6\,A. \tag{19}$$

Step 10. *Is the design feasible?*

The design is feasible only when the two inequality equations in Step 9 are simultaneously satisfied. If such a circumstance arises, the design procedure stops. Otherwise, stepwisely regress to Step 8, 7, 6 and 5, and modify the previous design.

After the final design has been determined, the other detailed mechanical structures

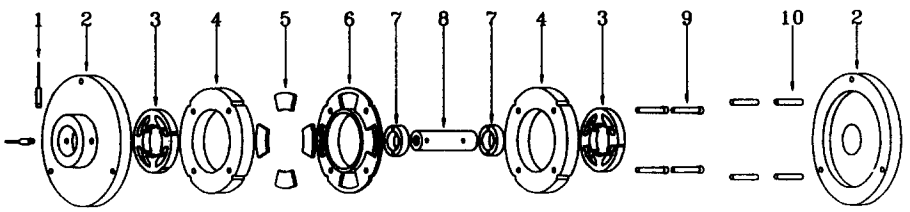

1 : Sensor probes
2 : Sensor probe seats
3 : EM stators
4 : Flux rings
5 : Rare earth permanent magnets
6 : Central ring
7 : Outer sleeves
8 : Inner sleeve
9 : Screws
10: Draw rods

FIG. 5. Exploded assembly drawing.

are then designed to make the prototype complete. Figure 5 shows an exploded assembly drawing of the final PEMB prototype. Two four-rib motor stators are included in each PEMB. Figure 2 shows the winding arrangement for one of the PEMBs; a similar winding scheme is used for another PEMB.

V. Auxiliary Devices for the PEMB Assembly

5.1. *Installation of the permanent magnets*

Because of the strong attraction force caused by PMs, when installing the PMs on the central ring they must be prevented from bumping against the flux ring. Moreover, since the hole on the central ring is precisely wire-cut, the axial PM dimension is thin, and the NdFeB PM is brittle, if a PM is pulled away from the central ring and attracted to the flux ring, separating the PM from the flux ring may be difficult without damaging the PM. If the PMs are damaged in this way, relocating them into the central ring would be difficult because of the high precision wire-cut PM location holes. The leakage flux provided by the PMs may also increase because of poor attachment between the PMs and the flux ring. To avoid these problems, an auxiliary device for setting up the permanent magnets was designed; Fig. 6 depicts the installation process, where the fixture and base plate are both made of aluminum to prevent attraction from the PMs. Notably, the central ring must be made of a non-magnetic material to reduce the flux leakage between PMs; aluminum alloy is chosen here.

5.2. *Alignment*

Proper alignment depends primarily on the precision of machining and the set-up methods. For this test rig, the PEMB seat, the backup bearing seat (i.e. the ball bearing seat), and the motor seat are located in the groove of the aluminum platform via sliding bricks. A series of holes is drilled on the platform to enable the location of these seats to be easily changed. A simple high precision test bar with small pins through it is

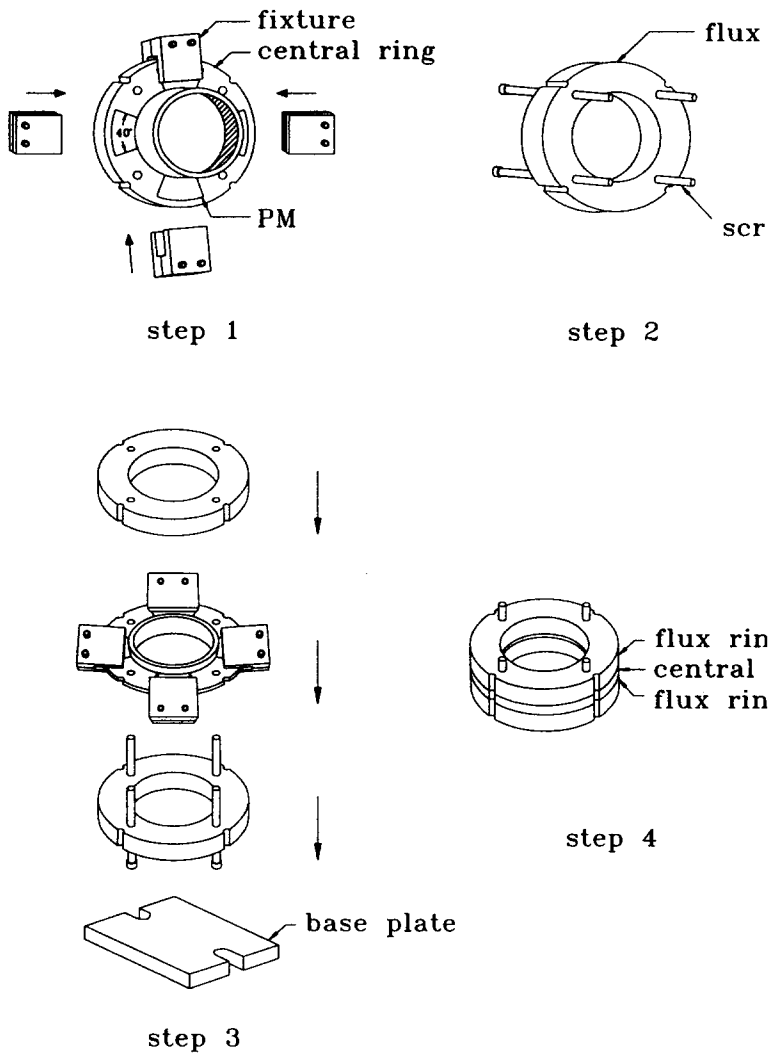

FIG. 6. The permanent magnet assembly.

designed to check the alignment of these seats. By inserting this test bar through the holes of the seats, the two backup bearing seats can be aligned because the backup bearings' diameter is nearly the same size as that of the test bar. First, move the test bar forward or backward so that the small pin on the test bar reaches the hole of the PEMB seat. Then, adjust the length of the pin so that it slightly touches one of the electromagnetic pole faces, and turn the test bar around. By feeling the change of tightness between one end of the pin and the electromagnetic pole faces, we can ensure that the two PEMB seats are aligned with the backup bearings. Notably, the pins do not need to be located at the center of the test bar; the only requirements are that the length of the pins be sufficiently long to touch the electromagnetic pole face and that the end face of the pins be as sharp as a needle.

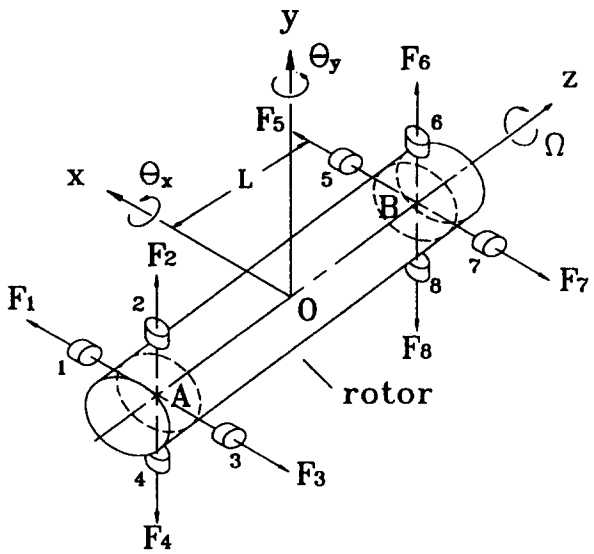

FIG. 7. Analytical model of the rotor-bearing system.

VI. System Model and Controller Design

6.1. *System model*

Figure 7 shows the analytical model for the PEMB controlled rotor-bearing system. The attractive force supplied by the electromagnet acting on the rotor is expressed as F_n ($n = 1 \sim 8$); the direction and action point of each force are also represented. Here the rotor is assumed to be rigid, symmetric and without mass unbalance. Furthermore, all displacements from the desired position are assumed to be small. Based on these assumptions, the displacement of the rotor mass center (point O in Fig. 7), i.e. x, y, θ_x and θ_y, can be expressed in terms of the movement at points A and B as follows:

$$x = \frac{x_1 + x_2}{2}, \quad \theta_x \cong \tan\theta_x = \frac{y_1 - y_2}{2L},$$

$$y = \frac{y_1 + y_2}{2}, \quad \theta_y \cong \tan\theta_y = \frac{x_2 - x_1}{2L}, \tag{20}$$

where x_1 and y_1 are the displacements at point A, x_2 and y_2 are the displacements at point B, and L is the distance between the rotor mass center and point A (or B). The input forces F_1–F_8 provided by the electromagnets can be linearized around the central position and represented as

$$F_n = k_d \cdot d_n + k_i \cdot i_n, \quad n = 1\text{–}8 \tag{21}$$

where k_d, k_i, d_r and i_n represent the displacement stiffness, the current stiffness, the change of air gap length corresponding to the electromagnet, and the coil current of electromagnet, respectively. From Eqs (20) and (21), the equation of motion of the rotor mass center can be expressed as

$$m\frac{\ddot{x}_1+\ddot{x}_2}{2}2k_d(x_1+x_2) = k_i(i_1-i_3+i_5-i_7),$$

$$m\frac{\ddot{y}_1+\ddot{y}_2}{2}2k_d(y_1+y_2) = mg+k_i(i_2-i_4+i_6-i_8),$$

$$I_r\frac{\ddot{x}_2-\ddot{x}_1}{2L^2}-\Omega I_a\frac{\dot{y}_1-\dot{y}_2}{2L^2}-2k_d(x_2-x_1) = k_i(-i_1+i_3+i_5-i_7),$$

$$I_r\frac{\ddot{y}_1-\ddot{y}_2}{2L^2}+\Omega I_a\frac{\dot{x}_2-\dot{x}_1}{2L^2}-2k_d(y_1-y_2) = k_i(i_2-i_4-i_6+i_8), \tag{22}$$

where m is the mass of the rotor, g is the acceleration of gravity, I_r is the transverse mass moment of inertia of the rotor, I_a is the polar mass moment of inertia of the rotor, and Ω is the rotor's rotating speed.

6.2. *Controller design*

A differential driving mode is adopted here, i.e. the currents flowing through the electromagnets are designed as $i_1 = -i_3$, $i_2 = i-_4$, $i_5 = -i_7$, and $i_6 = -i_8$. Furthermore, the coil current i_j, $j = 1$–8, consists of a static part i_{j0} and a dynamic part i_j^*, i.e. the controlled current. To provide an initial force to suspend the rotor, we set $i_{20} = -i_{40} = i_{60} = -i_{80} = mg/4k_i$ and $i_{10} = i_{30} = i_{50} = i_{70} = 0$. If $I_r/L^2 = m$ is selected, then the equations of motion (22) can be simplified and rewritten in matrix form as

$$\mathbf{M}\ddot{\mathbf{x}}+\mathbf{D}\dot{\mathbf{x}}+\mathbf{K}\mathbf{x} = \mathbf{B}\mathbf{u}, \tag{23}$$

where

$$\mathbf{M} = m\times\mathbf{I}_{4\times4},$$

$$\mathbf{D} = \frac{m\Omega I_a}{2I_r}\times\begin{bmatrix} 0 & 0 & 1 & -1 \\ 0 & 0 & -1 & 1 \\ -1 & 1 & 0 & 0 \\ 1 & -1 & 0 & 0 \end{bmatrix},$$

$$\mathbf{K} = -4k_d\times\mathbf{I}_{4\times4},$$

$$\mathbf{B} = 4k_i\times\mathbf{I}_{4\times4},$$

$$\mathbf{u} = [i_1^*\ i_5^*\ i_2^*\ i_6^*]^T,$$

$$\mathbf{x} = [x_1\ x_2\ y_1\ y_2]^T \equiv [x_1\ x_2\ x_3\ x_4]^T.$$

Table I lists the characteristic values of the open-loop system (23). From these characteristic values, the rotor-bearing system is known to be inherently unstable and, thus, a controller is necessary to make the system stable.

The control system controls the rotor's position by providing a current to the electromagnet based on the signals from the position sensors. The distance between the magnet poles and the shaft of the rotor is measured by the eddy current type position sensor. Signals from the position sensor are then compared with the reference signal,

TABLE I
Characteristic values of the open loop system with $\Omega = 1000$ *rad/s*

Characteristic values
−562.22+3.43i
−562.22−3.43i
562.22+3.43i
562.22−3.43i
−562.23
562.23
−562.23
562.23

which defines the rotor's center position. The error signal is proportional to the difference between the center position and the actual position of the rotor at any given time. If the error signal is zero, the rotor position is in the center of the stator. According to the error signal's magnitude, the controller generates a suitable low power control signal to the power amplifier and, then, the power amplifier supplies the control current to the winding coils so that suitable bearing forces are generated and the desired rotor position is maintained.

Two different structures for the multi-variable control system are the central control, which utilizes the complete state feedback and the decentralized control, where each bearing is controlled separately. Previous studies (**4, 11, 12**) indicate that the central feedback control matrix is extremely complicated and coupled with all states. The decentralized control eliminates the interconnection of states between the two PEMBs, and also the interconnection between the x- and y-direction states of a single PEMB. Thus for an analog control system, the hardware of the controller unit using the decentralized control structure is more easily realized.

Examining the second-order dynamic Eq. (23) reveals that position and velocity feedback control are necessary for the asymptotic stability of the entire system. The control law used here is expressed as

$$\mathbf{u} = \mathbf{K}_p\mathbf{x} - \mathbf{K}_d\dot{\mathbf{x}}, \tag{24}$$

where $\mathbf{K}_p$ and $\mathbf{K}_d$ are the position and velocity feedback control gain matrices, respectively. Here, a suitable position feedback control gain matrix $\mathbf{K}_p$ is selected to cause the matrix $\mathbf{K}+\mathbf{BK}_p$ to be symmetric and positive definite; in addition, the velocity feedback control gain matrix $\mathbf{BK}_d$ is allowed to be a symmetric and non-negative definite matrix (**13**).

The total energy stored in the system is the sum of kinetic and potential energy:

$$H = T+E = \tfrac{1}{2}\dot{\mathbf{x}}^T M\dot{\mathbf{x}} + \mathbf{x}^T(\mathbf{K}+\mathbf{BK}_p)\mathbf{x}. \tag{25}$$

Differentiating Eq. (25) with respect to time and using Eqs (23) and (24) yield

$$\dot{\mathbf{H}} = -\dot{\mathbf{x}}^{\mathrm{T}}\mathbf{B}\mathbf{K}_{\mathrm{d}}\dot{\mathbf{x}} < 0, \quad \text{for } \dot{\mathbf{x}} \neq 0 \tag{26}$$

since $\mathbf{B}\mathbf{K}_{\mathrm{d}}$ is symmetric and non-negative definite.

According to the Lyapunov stability theorem, the overall control system is an asymptotic stable system. Notably, the gyroscopic effect would not destroy the stability in such a particular choice of the position of magnetic bearings and shaft.

For the sake of simplicity and easy implementation, both $\mathbf{K}_{\mathrm{p}}$ and $\mathbf{K}_{\mathrm{d}}$ are set as diagonal matrices, or

$$\begin{aligned} \mathbf{K}_{\mathrm{p}} &= \mathrm{diag}(k_{\mathrm{p}1}k_{\mathrm{p}2}k_{\mathrm{p}3}k_{\mathrm{p}4}), \\ \mathbf{K}_{\mathrm{d}} &= \mathrm{diag}(k_{\mathrm{d}1}k_{\mathrm{d}2}k_{\mathrm{d}3}k_{\mathrm{d}4}). \end{aligned} \tag{27}$$

In this manner, the controllers of the four pairs of electromagnetics can be implemented independently. The control law is expressed as

$$u_j = -k_{\mathrm{p}j} \cdot x_j - k_{\mathrm{d}j} \cdot \frac{\mathrm{d}x_i}{\mathrm{d}t}, \quad j = 1\text{–}4. \tag{28}$$

Figure 2 shows the control circuit of one PEMB, where the compensated voltage from the controller is sent to the power amplifier to provide a suitable control current in the electromagnet winding and, thus, to control the rotor's position.

VII. Experimental Results and Discussion

Figure 8 presents the experimental set-up for the PEMB-suspension rotor. The rigid shaft, which is in 11-mm-diameter hardened high carbon steel rod 301 mm in length, has two sleeves, as indicated in Fig. 1. The sleeves are used for two magnetic bearings and four sensors, i.e. the magnets and sensors are collocated. This rotor's total mass is 0.823 kg and the gap length is 1.1 mm. The backup bearings provide protection in an emergency when the vibration amplitude exceeds 0.5 mm. The analog controllers consist of proportional and differential circuits. Moreover, the displacement stiffness k_{d} and the current stiffness k_i of the PEMB are obtained as 65,000 N/m and 13 N/A, respectively. The gains of the four PD-controllers are identical, i.e. $k_{\mathrm{p}j} = 10{,}000$ and $k_{\mathrm{d}j} = 5.5, j = 1\text{–}4$.

Table II lists the eigenvalues of the closed-loop system at different rotating speeds Ω. This table reveals that closed-loop stability is guaranteed even when the rotating speed Ω increases to infinity. Figure 9 shows a summary of the experimental results for the orbits of the rotor at low and high rotating speeds where the upper speed is limited by the rated speed of the rotor used. Although the orbit must theoretically decay to zero without any steady state error, the orbit would not be zero practically because of the existence of unbalance and misalignment in the rotor system. This figure indicates that the rotor's orbit at the left-hand PEMB (see Fig. 1) is larger than that at the right-hand PEMB. The larger orbit at the left-hand PEMB is due to a slight misalignment between the motor shaft and the rotor shaft. When the motor drives the motor, this alignment causes an exciting force acting on the rotor through the flexible coupling. Moreover, the orbit becomes smaller as the rotor's speed increases. At a low rotating speed ($\Omega \leqslant 3500$ rpm), the orbit at the left-hand PEMB is greater than one tenth of

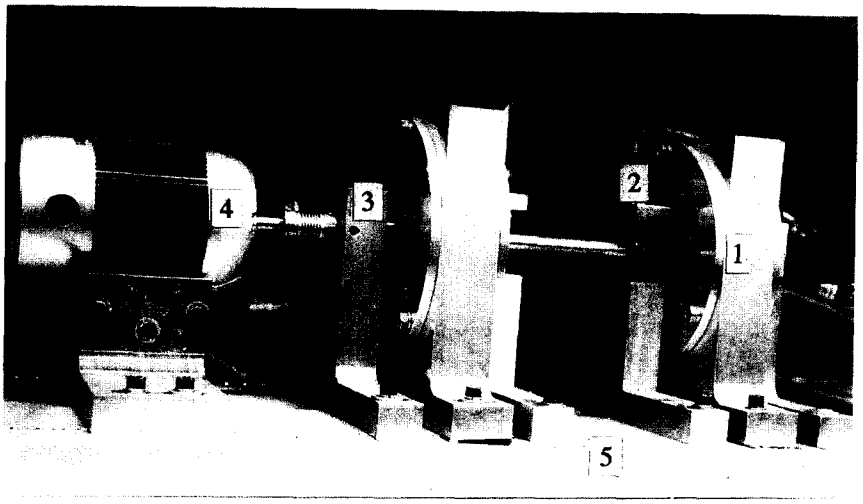

1 : Magnetic bearing
2 : Sensor
3 : Backup bearing
4 : Motor
5 : Platform

FIG. 8. Experimental setup of the magnetic suspension rotor.

the nominal gap length (0.1 mm). However, the orbit at the right-hand PEMB remains within one tenth of the gap length for all rotating speeds. These results reveal that the displacement of the rotor is maintained in an acceptably small range; meanwhile, the rotor speeds increase to a value of 12,000 rpm.

VIII. Conclusions

This study has not only developed a permanent-magnet-biased magnetic bearing, but has also applied it to control a rotor system. A systematic design procedure, capable of facilitating the design of the permanent/electromagnet magnetic bearing (PEMB), has also been proposed. Our experience in designing the PEMB shows that to have a high load capacity, the poles must have large cross-sectional areas to prevent saturation. By using permanent magnets to provide the bias flux, power consumption can be saved and the compact configuration can be obtained.

Also, a system model for analyzing the PEMB-rotor system is presented. By applying

TABLE II
Characteristic values of the closed loop system with $k_{pj} = 10{,}000$ *and* $k_{dj} = 5.5$; $j = 1$–4

Rotating speeds	Characteristic values
0 rad/s	$-175.37+524.61i$
	$-175.37-524.61i$
	$-175.37+524.61i$
	$-175.37-524.61i$
	$-175.37+524.61i$
	$-175.37-524.61i$
	$-175.37+524.61i$
	$-175.37-524.61i$
1000 rad/s	$-177.01+529.54i$
	$-177.01-529.54i$
	$-173.73+519.72i$
	$-173.73-519.72i$
	$-175.37+524.61i$
	$-175.37-524.61i$
	$-175.37+524.61i$
	$-175.37-524.61i$
∞ rad/s	$-350.74+\infty i$
	$-350.74-\infty i$
	0^-
	0^-
	$-175.37+524.61i$
	$-175.37-524.61i$
	$-175.37+524.61i$
	$-175.37-524.61i$

a decentralized state feedback control algorithm to the PEMB-rotor system, a relatively simple controller structure can be easily implemented. Experimental results indicate that the rotor deflection can be controlled within a small range and the rotor speed can be increased to a value of 12,000 rpm. These results illustrate the effectiveness of the proposed bearing system.

Acknowledgement

The authors would like to thank the National Science Council, Republic of China for financial support of this manuscript under Contract number NSC 81-0401-E-009-08.

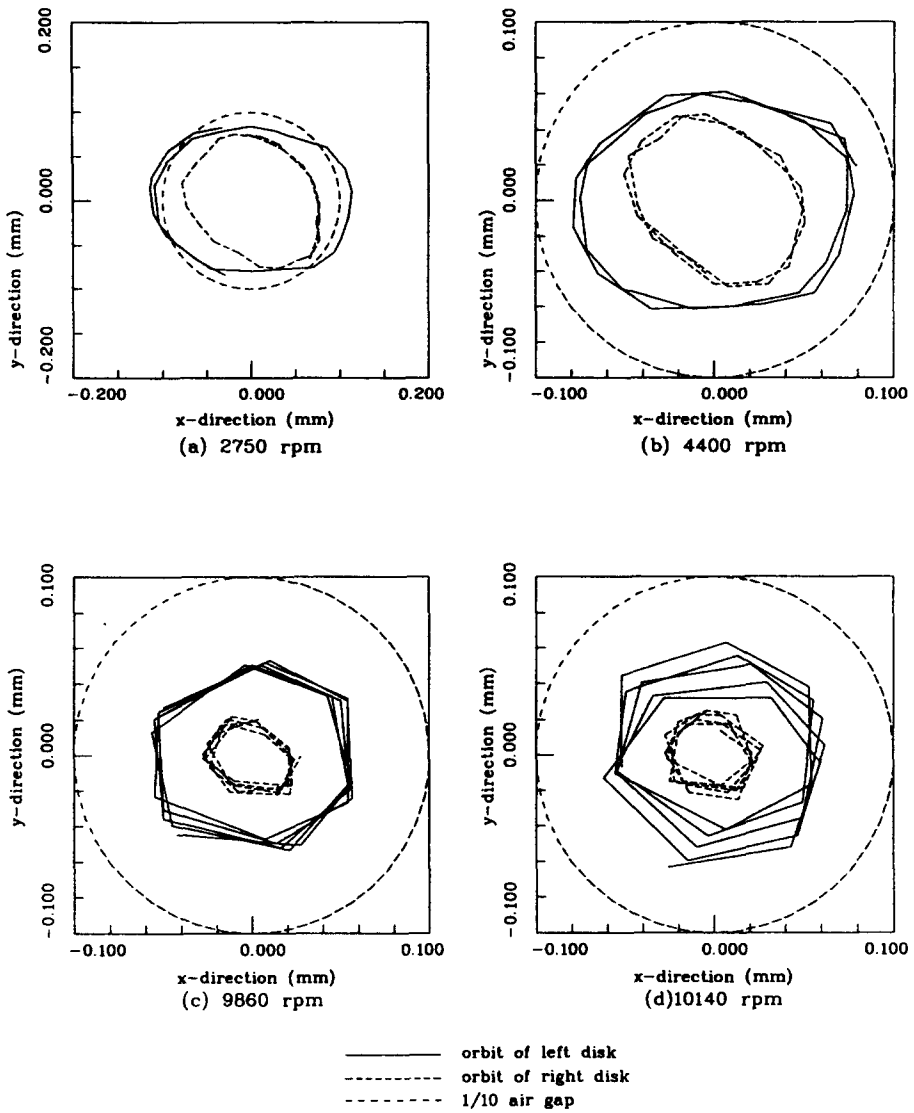

FIG. 9. The orbits of the rotor at different rotating speeds.

References

(1) R. D. Williams, F. J. Keith and P. E. Allaire, "Digital control of active magnetic bearings", *IEEE Tran. on Indus. Electrons*, Vol. 37, No. 1, p. 19, 1990.

(2) H. M. Chen and M. S. Darlow, "Magnetic bearing with rotating force control", *Trans. ASME, J. Tribology*, Vol. 110, p. 100, 1988.

(3) M. Hisatani, Y. Inoue and J. Mitsui, "Development of digitally controlled magnetic bearing", *Bull. JSME*, Vol. 29, No. 247, p. 214, 1984.

(4) T. Mizuno and T. Higuchi, "Design of the control system of totally active magnetic bearings", in "Int. Symp. on Design and Synthesis", Tokyo, 11–13 July, p. 534, 1984.

(5) A. C. Lee, F. Z. Hsiao and D. Ko, "Analysis and testing of a magnetic bearing with permanent magnets for bias", *JSME Int. J. Ser. C*, Vol. 37, No. 4, p. 774, 1994.
(6) J. M. Amiss, F. D. Jones and H. H. Ryffel, "Machinery's Handbook", 23 revised edition, Industrial Press Inc., New York, pp. 302–314, 1988.
(7) A. C. Lee, F. Z. Hsiao and D. Ko, "Performance limits of permanent magnet biased magnetic bearing", *JSME Int. J. Ser. C*, Vol. 37, No. 4, p. 783, 1994.
(8) C. D. Bradfield, J. B. Roberts and R. Karunendiran, "Performance of an electromagnetic bearing for the vibration control of a supercritical shaft", *Proc. Instn. Mech. Engrs*, Vol. 201 (C3), p. 201, 1987.
(9) J. L. Nikolajsen, R. Hulmes and V. Gondhalekar, "Investigation of an electromagnetic damper for vibration control of a transmission shaft", *Proc. Instn. Mech. Engrs*, Vol. 193, p. 331, 1979.
(10) L. Matsch and J. Morgan, "Electromagnetic and Electromechanical Machines", 3rd ed., Harper & Row, New York, pp. 46–52, 1986.
(11) N. Kenzou, N. Y. Takashi and T. Manabu, "Vibration and control of a flexible rotor supported by magnetic bearings", *JSME Int. J. Ser. III*, Vol. 33, No. 4, p. 475, 1990.
(12) M. Fumio, K. Mamoru and T. Yoshimi, "Design method of horizontal shaft attractive controlled magnetic bearing and its characteristics", *Elect. Engng in Japan*, Vol. 103, No. 3, p. 130, 1983.
(13) A. C. Lee and Y. H. Fan, "Decentralized control of a rotor system supported by magnetic bearings", *Int. J. Mach. Tools Manufact.*, Vol. 35, No. 3, p. 445, 1995.